Size dependence of the electronic structures and electron-phonon coupling in ZnO quantum dots

S. C. Ray, Y. Low, H. M. Tsai, C. W. Pao, J. W. Chiou,[a] S. C. Yang, F. Z. Chien, and W. F. Pong[b]
Department of Physics, Tamkang University, Tamsui 251, Taiwan

M.-H. Tsai
Department of Physics, National Sun Yat-Sen University, Kaohsiung 804, Taiwan

K. F. Lin, H. M. Cheng, and W. F. Hsieh
Department of Photonics and Institutes of Electro-Optical Engineering, National Chiao Tung University, Hsinchu 300, Taiwan

J. F. Lee
National Synchrotron Radiation Research Center, Hsinchu 300, Taiwan

(Received 21 October 2007; accepted 21 November 2007; published online 26 December 2007)

The electronic structures and optical properties of various sizes of ZnO quantum dots (QDs) were studied using x-ray absorption, photoluminescence, and Raman spectroscopy. The increase in the intensity ratio of the second-order Raman spectra of longitudinal optical mode and its fundamental mode, which is related to the strength of the electron-phonon coupling (EPC), is found to increase with the size of QD. The trend of EPC also correlates with the increase of the intensity ratio of the O $2p_\pi$ (I_π) and $2p_\sigma$ (I_σ) orbital features in the O *K*-edge x-ray absorption near-edge structure (XANES) as the size of QD increases. The EPC and XANES results suggest that the crystal orientations of ZnO QDs are approximately aligned with the *c* axis parallel with the polarization of x-ray photons. © *2007 American Institute of Physics*. [DOI: 10.1063/1.2824396]

Electron-phonon coupling (EPC) in nanomaterials has attracted much attention in the past years because great interest exists to elucidate its fundamental physics and potential applications.[1–3] The increase of the strength of EPC with the size of the nanostructures substantially influences the electrical and optical properties of these materials. Recently, Cheng *et al.* and Lin *et al.* investigated the size dependence of the optical properties and EPC of ZnO quantum dots (QDs) using photoluminescence (PL) and Raman spectroscopy.[4–6] However, the dependence of the strength of EPC on the size of the nanomaterials is still not well understood.[1–6] In contrast, the anomalous blueshift of the luminescence emission spectra of ZnO nanorods/nanowires with the decrease of their diameters, which are far beyond the quantum confinement regime, has been understood to be caused by the surface effect associated with the increased surface-to-volume ratio.[7] The calculation from first principles may further provide a theoretical basis for understanding the observed shift in the emission spectra of nanomaterials.[8] The nanostructures of ZnO are inherently asymmetric, so that their orientations strongly affect their x-ray absorption and optical properties.[9] Despite many phenomenological studies, the origin of the shift in phonon frequency and carrier recombination in ZnO nanomaterials remain the subjects of much debates.[10,11] This work focuses on the understanding of the relationship between the electronic structures revealed by the x-ray absorption near-edge structure (XANES), the extended x-ray absorption fine structure (EXAFS), and the observed ultraviolet (UV)-PL and resonant Raman spectroscopy spectra, in particular the peak shift in the spectra and size-dependent EPC in ZnO QDs.

Zn L_3-, Zn *K*-, and O *K*-edge XANES and Zn *K*-edge EXAFS spectra were obtained at the National Synchrotron Radiation Research Center in Hsinchu, Taiwan. The room-temperature UV-PL and resonant Raman spectroscopy were performed using a He–Cd laser with a wavelength of 325 nm. ZnO QDs were synthesized using the sol-gel method and their mean sizes were tuned by controlling the concentration of zinc precursor, as described elsewhere.[4–6] Three ZnO QD samples with diameters of ~6, 12, and 20 nm were determined by transmission electron microscopy (TEM). In Fig. 1, the upper inset shows TEM images of the

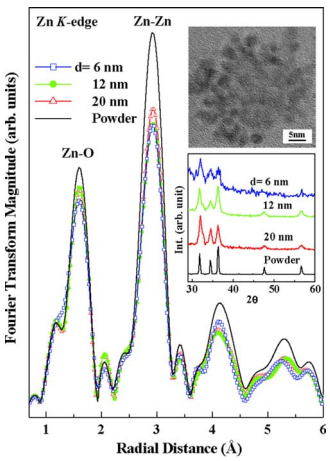

FIG. 1. (Color online) Magnitude of FT of EXAFS $k^3\chi$ data at the Zn *K*-edge of all ZnO QDs and powder. TEM image of 6 nm QDs (upper inset) and the XRD spectra (lower inset) of ZnO QDs and powder.

[a]Permanent address: Department of Applied Physics, National University of Kaohsiung, Taiwan.

[b]Author to whom correspondence should be addressed. On leave at: Advanced Light Source, Lawrence Berkeley National Laboratory, Berekeley, California. Electronic mail: wfpong@mail.tku.edu.tw.

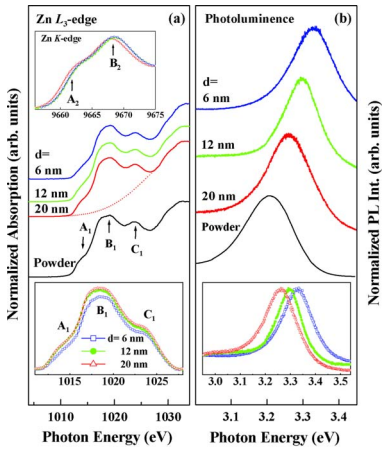

FIG. 2. (Color online) (a) Zn L_3-edge XANES spectra of all ZnO QDs and powder. Lower inset displays magnified Zn L_3-edge features following background subtraction and the upper inset displays the Zn *K*-edge XANES spectra. (b) Room-temperature UV-PL spectra of all ZnO QDs. Inset shows the shifts of the PL spectra.

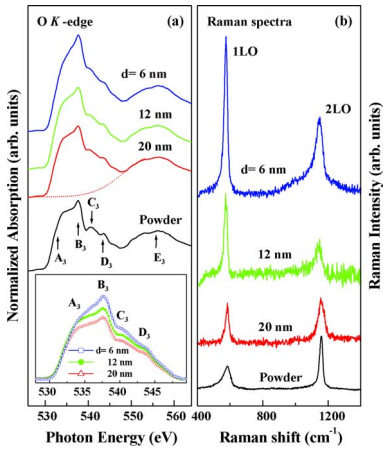

FIG. 3. (Color online) (a) O *K*-edge XANES spectra of all ZnO QDs and powder. Inset displays magnified O *K*-edge features following background subtraction. (b) Resonant Raman scattering spectra of all ZnO QDs and bulk ZnO (Ref. 18).

6 nm QDs and the lower inset shows x-ray diffraction (XRD) spectra of all QDs and the ZnO powder. TEM reveals that QDs are essentially small spheroids/ellipsoids and XRD indicates the presence of a hexagonal (wurtzite) structure in QDs such as the ZnO powder. Figure 1 also displays the Fourier transform (FT) of Zn *K*-edge EXAFS $k^3\chi$ data of ZnO QDs and powder. It reveals that the general line shape and the radial distribution of the FT spectra of QDs are almost identical to those of the powder, which demonstrates that the local atomic structures of Zn atoms in ZnO QDs and powder are similar. Notably, the intensities of the first two main peaks in the FT spectra, corresponding to the nearest-neighbor (NN) Zn–O and next-nearest-neighbor (NNN) Zn–Zn bond lengths,[12] decrease with the decrease of the size of QD and are remarkably smaller than those of the powder. The FT spectra are further analyzed by a combination of the multiple-scattering EXAFS computer program FEFF code[13] and the nonlinear least-squares-fitting computer program FEFFIT. In NN Zn–O and NNN Zn–Zn coordination shells, the coordination numbers (4 and 12) and bond lengths (1.98 ± 0.01 and 3.24 ± 0.02 Å) were almost identical for all ZnO QDs and powder. However, the Debye-Waller factors of the NN Zn–O coordination shell increased in the order of $\sim 4.7\times10^{-3}$ Å^2 for powder, 5.7×10^{-3} for 20 and 12 nm QDs, and 6.3×10^{-3} Å^2 for 6 nm QD, and those of the NNN Zn–Zn coordination shell increased in the order of $\sim 8.4\times10^{-3}$ Å^2 for powder, 1.0×10^{-2} for 20 nm QD, and 1.1×10^{-2} Å^2 for 12 and 6 nm QDs. The trend suggests an increase of the structural disorder around Zn sites, which is probably due to the increase of the number of dangling bonds/surface states as the size of QD decreases.

Figure 2(a) shows Zn L_3-edge XANES spectra of ZnO QDs and powder. Features A_1 ($\sim$1014 eV), B_1 ($\sim$1019 eV), and C_1 ($\sim$1023 eV) in Fig. 2(a) are associated with the transition of Zn $2p$ electrons to unoccupied Zn $4sd$ states.[14,15] The inset at the bottom of Fig. 2(a) is a magnified view of the near-edge features after the background has been subtracted using a best-fitted Gaussian curve indicated by the dotted line. The overall intensities of features A_1–C_1 decrease as the size of QD decreases, indicating that the number of unoccupied Zn $4sd$ states near the conduction-band minimum is reduced as the size of QD decreases. In contrast, the number of Zn $4p$ unoccupied states increases and decreases, respectively, for features B_2 and A_2 as the size of QD decreases, as shown in the inset at the top of Fig. 2(a). The absorption edge is also observed to be shifted slightly to the higher energy side in both Zn *K*- and L_3-edge XANES spectra as the size of QD decreases from 20 to 6 nm. As the size of ZnO QD decreases, the QD becomes nearly spherical.[16] The intensities of features B_2 and A_2 are enhanced and suppressed, respectively, which may correspond to the shift of unoccupied Zn $4p$ states in region A_2 to higher energy region B_2 due to the increase of the band gap. This finding is consistent with the results of an earlier work of diameter-dependent ZnO nanorods.[15] Figure 2(b) presents UV-PL spectra of ZnO QDs and powder and the inset displays relative positions of these PL spectra of QDs, revealing the shift of the PL-maximum from $\sim$3.26 eV (20 nm) to 3.33 eV (6 nm). However, the shifts of PL peaks of nanomaterials can principally be attributed to excitonic transitions, surface effects, quantum confinement effect, surface impurities/defects, and bulk defects such as oxygen vacancies.[16,17] In the present case, the quantum confinement effect and bulk defects may not be the cause, because the sizes (6–20 nm) are larger than the exciton Bohr radius (1–2 nm) (Ref. 16) and green luminescence is absent in ZnO QDs PL spectra. Thus, the change of the excitonic transition due to the variation of electronic density of states and surface effects are primarily responsible for the shifts of the PL peak and the Zn L_3- and *K*-edge XANES features toward higher energy as the size of QD decreases.

Figure 3(a) displays the O *K*-edge XANES spectra of ZnO QDs and powder. The O *K*-edge spectra reveal that the intensities of features A_3–E_3 of QDs are similar to those of the reference powder. Features A_3–E_3 are associated with electron excitations from O $1s$ to O $2p_\pi$ and $2p_\sigma$ states.[14,15] Angle-dependent XANES measurements and theoretical calculations have identified that features A_3 ($\sim$535.2 eV) and B_3 ($\sim$537.6 eV) primarily correspond to the excitation of an O $1s$ electron to $2p_\pi$ and $2p_\sigma$ orbitals,[9] respectively. The $2p_\pi$ bonds lie along the *c* axis, while the $2p_\sigma$ bonds lie approximately perpendicular to the *c* axis of QDs. The overall intensities of features A_3 and B_3 increase as the size of ZnO QD decreases, which may reflect the increase of the unoccupied dangling bond/surface states due to the increase of the

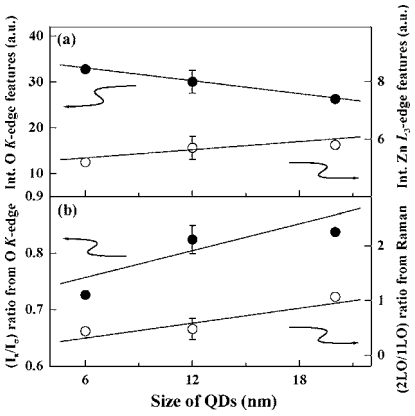

FIG. 4. (a) Integrated intensities of O *K*-edge (filled circles) and Zn L_3-edge (open circles) XANES features. (b) The intensity ratio between the second- and first-order Raman scattering cross sections 2LO/1LO (open circles) and the intensity ratio between the O $2p_\pi$ and $2p_\sigma$ orbital features I_π/I_σ (filled circles).

surface-to-volume ratio. Figure 3(b) presents the resonant Raman spectra of ZnO QDs and the reference bulk ZnO (the reference spectrum is taken from another study[18]). This figure revealed that both first-order (at ~577 cm^{-1}) and second order (overtone at ~1150 cm^{-1}) longitudinal optical phonon modes (denoted as 1LO and 2LO) are enhanced as QDs are downsized to 6 nm, because both modes are superposition of the LO phonon mode in which Zn and O atoms moves in the same direction in a unit cell. The enhancement of the LO phonon mode suggests an *n*-phonon-process contribution to the Raman cross section,[5] which occurs when incoming or scattered photon matches the energy difference of two electronic states. However, regardless of the enhancement, the ratio of the intensities of the second- and first-order Raman scattering cross sections of the LO mode, denoted as 2LO/1LO, was argued to be related to the strength of EPC.[3–5]

Figure 4(a) plots the integrated intensities of the O *K*- and Zn L_3-edge XANES features between 524–549 and 1010–1027 eV, which represent the numbers of O 2*p* and Zn 4*sd* unoccupied states, respectively, and vary inversely with the size of QD. The decrease of the number of Zn 4*sd* unoccupied states as the size of QD decreases suggests a reduction of Zn 4*sd*-O 2*p* antibonding coupling as QDs become smaller. In contrast, the overall intensity of the O *K*-edge XANES features increases as the size of QD decreases. The diameter-dependent ZnO nanorods exhibit a similar trend.[15] Figure 4(b) plots the 2LO/1LO intensity ratio, which increases from 0.44 to 1.07 with the increase of the ZnO QD size from 6 to 20 nm. The LO Raman scattering cross section is contributed principally from both the deformation and Fröhlich potentials, which involves a long-range interaction with the oscillating macroscopic electric field associated with the LO phonons.[19] The increase of the 2LO/1LO intensity ratio with the increase of the QD size, as presented in Fig. 4(b), is mainly related to the Fröhlich interactions.[3–5] More recently, Hsu *et al.* have proposed that the strength of EPC and the exciton Bohr radius are reduced due to the less polar nature of smaller sized QDs.[20] This behavior of EPC correlates with the increase of the O $2p_\pi$ $(I_\pi)/2p_\sigma$ (I_σ) orbital intensity ratio in the O *K*-edge XANES spectra as the size of QD increases, as also shown in Fig. 4(b). The enhancement of the Raman scattering cross section was argued to be due to a strong internal electric field given rise by piezoelectric and polarization effects of the ionic ZnO QDs in the wurtzite structure.[2] The I_π/I_σ ratio increases because the highly directional $2p_\pi$ orbitals lie along the *c* axis of QDs. Note that the x-ray absorption dipole transition probability is proportional to the absolute square of the dipole transition matrix $\langle\Psi_f|\mathbf{E}\cdot r|\Psi_i\rangle$ between the initial state Ψ_i(O 1*s*) and the final state Ψ_f(O $2p_\pi$), where **E** is the x-ray electric polarization vector **E** and ***r*** is the position vector operator. The magnitude of this matrix element is largest when the directional Ψ_f(O $2p_\pi$) orbital is parallel with **E**. For the 6 nm QDs with a more or less spherical shape and a larger surface-to-volume ratio, the distortion and rearrangement of Zn–O bonds near the surface cause alignment between O $2p_\pi$ orbitals and **E** to become poor and consequently a reduction of the overall dipole transition probability. As the size of QD increases the dots become more like *c* axis oriented rods rather than spheres. In conjunction with the reduction of the ratio of the distorted surface region to bulklike interior region, the alignment between O $2p_\pi$ orbitals and ***E*** is improved with the increase of the QD size, so does the dipole transition probability. Thus, the O $1s \rightarrow 2p_\pi$ transition is enhanced. The radiative de-excitation of O $2p_\sigma$ states are much less efficient, since the directional O $2p_\sigma$ orbitals are approximately perpendicular to the *c* axis. The results of Raman scattering are very similar to those of x-ray absorption of ZnO QDs when the x-ray electric polarization vector is parallel to the *c* axis.

[1] H. D. Sun, T. Makino, N. T. Tuan, Y. Segawa, M. Kawasaki, A. Ohtomo, K. Tamura, and H. Koinuma, Appl. Phys. Lett. **78**, 2464 (2001).
[2] S. Kalliakos, X. B. Zhang, T. Taliercio, P. Lefebvre, B. Gil, N. Grandjean, B. Damilano, and J. Massies, Appl. Phys. Lett. **80**, 428 (2002).
[3] R. P. Wang, G. Xu, and P. Jin, Phys. Rev. B **69**, 113303 (2004).
[4] H. M. Cheng, K. F. Lin, H. C. Hsu, C. J. Lin, L. J. Lin, and W. F. Hsieh, J. Phys. Chem. B **109**, 18385 (2005).
[5] H. M. Cheng, K. F. Lin, H. C. Hsu, and W. F. Hsieh, Appl. Phys. Lett. **88**, 261909 (2006).
[6] K. F. Lin, H. M. Cheng, H. C. Hsu, and W. F. Hsieh, Appl. Phys. Lett. **88**, 263117 (2006).
[7] C. W. Chen, K. H. Chen, C. H. Shen, A. Ganguly, L. C. Chen, J. J. Wu, H. I. Wen, and W. F. Pong, Appl. Phys. Lett. **88**, 241905 (2006).
[8] M.-H. Tsai, Z. F. Jhang, J. Y. Jiang, Y. H. Tang, and L. W. Tu, Appl. Phys. Lett. **89**, 203101 (2006).
[9] R. A. Rosenberg, G. K. Shenoy, L.-C. Tien, D. Norton, S. Pearton, X. H. Sun, and T. K. Sham, Appl. Phys. Lett. **89**, 093118 (2006).
[10] V. A. Fonoberov, K. A. Alim, A. A. Balandin, F. Xiu, and J. Liu, Phys. Rev. B **73**, 165317 (2006).
[11] B. Kumar, H. Gong, S. Y. Chow, S. Tripathy, and Y. Hua, Appl. Phys. Lett. **89**, 071922 (2006).
[12] S.-W. Han, H.-J. Yoo, S. J. An, J. Yoo, and G.-C. Yi, Appl. Phys. Lett. **86**, 021917 (2005).
[13] A. L. Ankudinov, B. Ravel, J. J. Rehr, and S. D. Conradson, Phys. Rev. B **58**, 7565 (1998).
[14] J. W. Chiou, J. C. Jan, H. M. Tsai, C. W. Bao, W. F. Pong, M.-H. Tsai, I.-H. Hong, R. Klauser, J. F. Lee, J. J. Wu, and S. C. Liu, Appl. Phys. Lett. **84**, 3462 (2004).
[15] J. W. Chiou, K. P. Krishna Kumar, J. C. Jan, H. M. Tsai, C. W. Bao, W. F. Pong, F. Z. Chien, M.-H. Tsai, I.-H. Hong, R. Klauser, J. F. Lee, J. J. Wu, and S. C. Liu, Appl. Phys. Lett. **85**, 3220 (2004).
[16] V. A. Fonoberov and A. A. Balandin, J. Nanoelectron. Optoelectron. **1**, 19 (2006).
[17] L. Guo, S. Yang, C. Yang, P. Yu, J. Wang, W. Ge, and G. K. L. Wong, Appl. Phys. Lett. **76**, 2901 (2000).
[18] J. F. Scott, Phys. Rev. B **2**, 1209 (1970).
[19] R. H. Callender, S. S. Sussman, M. Selders, and R. K. Chang, Phys. Rev. B **7**, 3788 (1973).
[20] W. T. Hsu, K. F. Lin, and W. F. Hsieh, Appl. Phys. Lett. **91**, 181913 (2007).